and D. L. Anderson, *J. Geophys. Res.* **94**, 1895 (1989); D. L. Anderson, *ibid.* **93**, 4688 (1988); C. Bina and B. J. Wood, *ibid.* **92**, 4853 (1987); D. J. Weidner, in *Chemistry and Physics of Terrestrial Planets*, S. K. Saxena, Ed. (Springer-Verlag, New York, 1986), pp. 251–274; S. M. Rigden, G. D. Gwanmesia, J. D. FitzGerald, I. Jackson, R. C. Liebermann, *Nature* **354**, 143 (1991)].

2. J. M. Brown, L. J. Slutsky, K. A. Nelson, L.-T. Cheng, *J. Geophys. Res.* **94**, 9485 (1989).
3. Elastic constants are elements of a second-order tensor relating the six independent components of stress to those of infinitesimal strain. Various relationships reduce the number of required elastic constants to nine for a mineral of orthorhombic symmetry.
4. M. D. Fayer, *IEEE J. Quantum Electron.* **22**, 1444 (1986); Y. X. Yan, L.-T. Cheng, K. A. Nelson, in *Advances in Non-Linear Spectroscopy*, J. H. Clark and R. E. Hester, Eds. (Wiley, London, 1987), pp. 1437–1452; K. A. Nelson, R. Casalegno, R. J. Dwayne Miller, M. D. Fayer, *J. Chem. Phys.* **77**, 1144 (1982); J. M. Brown, L. J. Slutsky, K. A. Nelson, L.-T. Cheng, *Science* **241**, 65 (1988).
5. J. M. Zaug, E. H. Abramson, J. M. Brown, L. J. Slutsky, in *High Pressure Research: Applications to Earth and Planetary Sciences*, Y. Syono and M. H. Manghnani, Eds. (American Geophysical Union, Washington, DC, 1992), pp. 157–166.
6. Y. Kudoh and Y. Takeuchi, *Z. Kristallogr.* **171**, 291 (1985).
7. We use the Hashin-Shtrikman bounds [P. J. Watt, *J. Appl. Phys.* **50**, 6290 (1979)].
8. The conversion from pressure to depth is based on seismic model PREM [A. M. Dziewonski and D. L. Anderson, *Phys. Earth Planet. Inter.* **25**, 297 (1981)].
9. S. Webb, *Phys. Chem. Minerals* **16**, 684 (1989).
10. M. Kumazawa and O. L. Anderson, *J. Geophys. Res.* **74**, 5961 (1969).
11. D. G. Isaak, *ibid.* **97**, 1871 (1992).
12. A. Chopelas, *Phys. Chem. Minerals* **17**, 149 (1990).
13. M. Born and K. Huang, *Dynamical Theory of Crystal Lattices* (Clarendon, Oxford, 1954).
14. B. H. Hager, M. A. Richards, R. P. Cormer, A. M. Dziewonski, *Nature* **313**, 541 (1985).
15. S. P. Grand and D. V. Helmberger, *Geophys. J. R. Astron. Soc.* **76**, 399 (1984).
16. M. C. Walck, *ibid.*, p. 697.
17. ——, *ibid.* **81**, 243 (1985).
18. X.-D. Li, D. Giardini, J. H. Woodhouse, *Geophys. J. Int.* **105**, 649 (1991).

19. Partial support for this work was provided by the National Science Foundation (grant EAR-8804897). Additional support was provided by the University of Washington (Chemistry Department, Geophysics Program, College of Arts and Sciences). A Chevron Graduate Fellowship (J.M.Z.) is also acknowledged.

12 November 1992; accepted 19 April 1993

Direct Imaging of the Diacetylene Solid-State Monomer-Polymer Phase Transformation

Jun Liao and David C. Martin*

The solid-state phase transformation from 1,6-di(*N*-carbazolyl)-2-4-hexadiyne (DCHD) diacetylene monomer to polymer has been studied dynamically by low-dose selected area electron diffraction and high-resolution electron microscopy. The total exposure required to induce polymerization is five orders of magnitude smaller than the critical dose for electron beam damage. The phase transformation is quasi-homogeneous, with the lattice parameters changing continuously as a function of beam dose. Characteristic streaking that develops in the selected area electron diffraction patterns in the [200] reciprocal directions during the intermediate stages of the transformation provides information about the defect-mediated mechanisms of this reaction.

In the last two decades, the lattice-controlled solid-state polymerization of diacetylenes has attracted considerable attention. This route can be used to prepare crystals of poly(diacetylenes) of macroscopic size with the chains in an extended conformation (*1*). These single crystals of fully conjugated macromolecules have become model materials for investigating the physics of one-dimensional optical and electrical phenomena in organic polymers (*2*). The mechanisms of the phase transformation from diacetylene monomer to polymer have been examined by x-ray diffraction (*3–6*), x-ray topography (*7, 8*), and polarized optical microscopy (*5*). Thermal polymerization is usually found to be heterogeneous, whereas radiation polymerization by ultraviolet light, γ-rays, or x-rays is often homogeneous. The intermediate transition states between monomer and polymer have also been studied by x-ray diffraction (*3–5*). However, because of the limited resolution of these techniques, the manner in which the phase transformation proceeds at the molecular level has remained unclear.

High-resolution information about materials structure is usually obtained by selected area electron diffraction (SAED) and high-resolution electron microscopy (HREM). Dynamic SAED and HREM are commonly used for studying inorganic systems (*9*). However, as is typical for organic materials, diacetylene monomers and polymers are sensitive to electron beam damage. Nevertheless, direct imaging by transmission electron microscopy (TEM) has been used in characterizing defects in certain polydiacetylene systems (*10–12*).

In the present study, we used the electron beam in the TEM to induce the monomer-polymer phase transformation in DCHD. We imaged this solid-state process in situ as a function of dose in a JEOL 400-kV high-resolution electron microscope equipped with a Gatan yttrium-aluminum-garnet (YAG) crystal video recording system and image intensifier (*13*). Both the DCHD monomer and polymer crystals are monoclinic: the monomer has a space group of $P2_1/c$ with $a = 1.760$ nm, $b = 1.360$ nm, $c = 0.455$ nm, and $\gamma = 94.0°$; the polymer has the same space group with $a = 1.739$ nm, $b = 1.289$ nm, $c = 0.490$ nm, and $\gamma = 108°$ (*14*). We follow the convention for crystalline polymers in which the chain direction is parallel to the *c* axis.

The most critical factor in conducting this dynamic observation is the electron dose required to transform the monomer to polymer (J_{mp}). We determined J_{mp} by measuring the change in the electron diffraction pattern as a function of time at a given electron beam current on the sample and magnification (*15*). For DCHD, we found J_{mp} to be 1×10^{-4} C cm^{-2} at 400 kV, which is five orders of magnitude smaller than the critical end-point dose J_c measured as 20 C cm^{-2} at 200 kV for the $0\bar{1}0$ reflection (*11, 16, 17*). Extraordinary care must be taken to reduce the incident dose rate and avoid illuminating the sample with any more electrons than are absolutely necessary.

By selecting different condenser aperture sizes and electron beam spot sizes, we were able to control the electron dose rate on the samples at 1×10^{-5} C cm^{-2} s^{-1}. Under these conditions, it takes 10 s for the DCHD monomer to be transformed into the polymer by the electron beam, which provides enough time to image the intermediate states of the transformation in detail with SAED. Recording an HREM image is possible with a spot size just sufficient to illuminate the YAG crystal (25 mm in diameter). This procedure minimizes the electron dose on the samples and makes it convenient to prefocus on an area adjacent to the area of interest in the minimum dose system. It also makes it possible to monitor the HREM images dynamically and record them on video tape. Our videos were digitized with a Scion video image 1000 board on a Mac II and analyzed by the "Image" processing program (*18*).

Molecular projections of the DCHD monomer and polymer in the [001] directions are shown in Fig. 1, A and F, respectively. A series of SAED patterns showing how the corresponding reciprocal lattices change during the monomer-polymer phase transformation are shown in Fig. 1, B to E. Figure 1B was taken at the beginning of the transformation and indexed as the [001] zone of the DCHD monomer. The pattern started to change at $J = 1 \times 10^{-5}$ C cm^{-2}, when γ increased and the lattice parameters *a* and *b* decreased. At *J*

Department of Materials Science and Engineering, College of Engineering, University of Michigan, Ann Arbor, MI 48109–2136.

*To whom correspondence should be addressed.

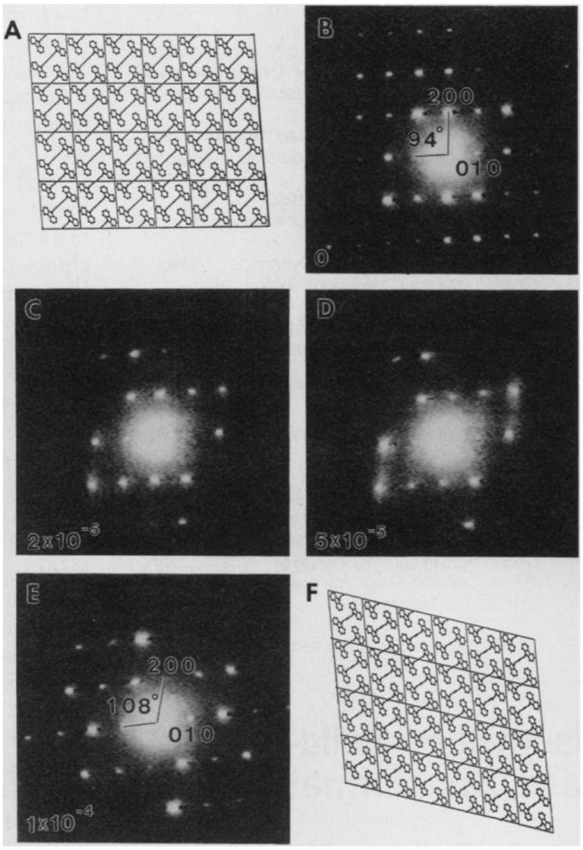

Fig. 1. (**A**) The molecular projection of the DCHD monomer in the [001] direction. (**B** to **E**) A series of SAED patterns showing the change of the DCHD reciprocal lattice during the phase transformation. The image in (B) was taken at $J \cong 0$ C cm^{-2}, corresponding to the [001] zone of the DCHD monomer. The pattern started to change at $J = 1 \times 10^{-5}$ C cm^{-2}, at which point γ increased and the lattice parameters a and b decreased. The image in (C) at $J = 2 \times 10^{-5}$ C cm^{-2} revealed that the diffraction spots started to streak along the [200] reciprocal lattice direction. The streaking increased in intensity until it reached a maximum at $J = 5 \times 10^{-5}$ C cm^{-2}, as shown in (D); after this dose, the streaking started to fade away, disappearing completely after $J = 1 \times 10^{-4}$ C cm^{-2}, as shown in (E). (**F**) The molecular projection of the DCHD polymer in the [001] direction.

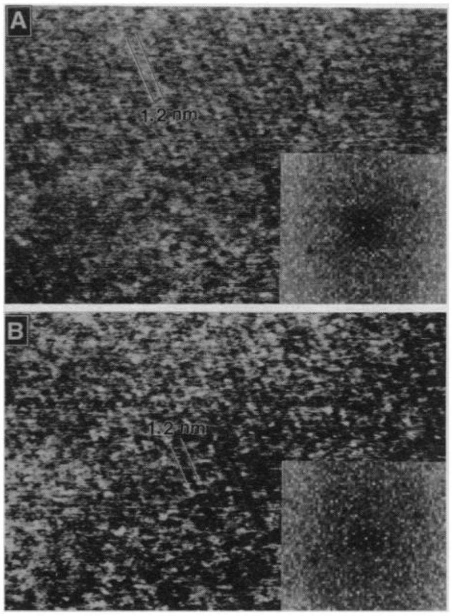

Fig. 3. Examples of HREM images of the DCHD lattice during the phase transformation showing the 1.2-nm (010) lattice image moving from the upper left in (**A**) down toward the middle in (**B**). The HREM images confirm that crystallinity is retained during the monomer-polymer phase transformation. The insets in (A) and (B) are the fast Fourier transforms obtained from these lattice images.

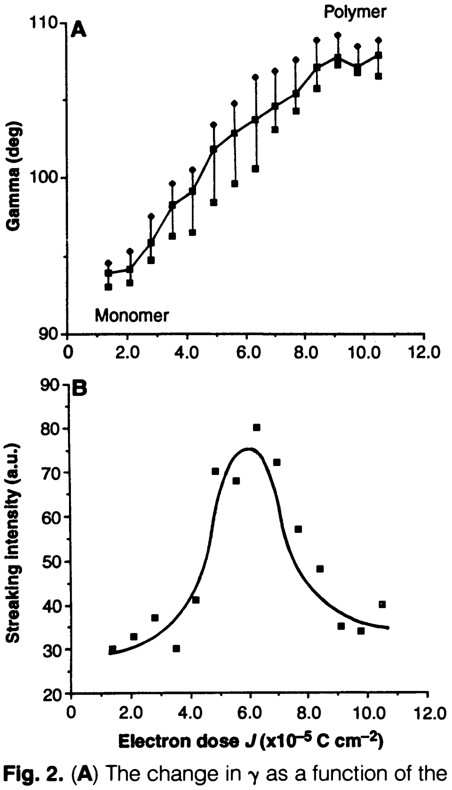

Fig. 2. (**A**) The change in γ as a function of the electron dose. The error bars were obtained by measurement of the FWHM of each spot. The most severe fluctuations occurred at 5×10^{-5} C cm^{-2}. (**B**) The change of streaking intensity (in atomic units) between the 200 and 020 spots as a function of the electron dose, showing the intensity maximum at 5×10^{-5} C cm^{-2}.

$= 2 \times 10^{-5}$ C cm^{-2} (Fig. 1C), the diffraction spots started to streak along the [200] reciprocal lattice direction. The streaking increased in intensity until it reached a maximum at $J = 5 \times 10^{-5}$ C cm^{-2} (Fig. 1D). For higher doses, the streaking started to fade away. The streaking faded away completely after $J = 1 \times 10^{-4}$ C cm^{-2} (Fig. 1E).

The curve in Fig. 2A shows the change of γ as a function of electron dose. The angle γ increased by 14° as expected from the crystal structures of the DCHD monomer and polymer (*14*). The (200) and (010) spots approached each other and rotated 10° and 4°, respectively, about the transmission spot. We examined the disorder induced during the transformation by measuring the full width at half maximum (FWHM) of each spot as a function of the dose. The (200), (020), and (220) spots all spread, reached their maxima in FWHM at the intermediate stages and shrank back at the final stage of the transformation. This spot broadening also leads to a distribution in γ, as shown by the error bars in Fig. 2A.

The appearance of the [200] streaking represents two-dimensional defects perpendicular to the [200] reciprocal direction induced during the transformation. The change of the streaking intensity corresponds to the change in the population of these two-dimensional defects. By measuring the diffraction intensity in the area of reciprocal space between the (220) and (020) spots, we found that the streaking intensity reached its maximum at $J = 5 \times 10^{-5}$ C cm^{-2} (Fig. 2B), which indicates that the most severe disorder induced by the phase transformation occurs at the middle stage of the reaction.

Our dynamic SAED studies indicate that the electron beam–induced transformation of DCHD monomer to polymer is quasi-homogeneous. The electron diffraction pattern is always a single crystal pattern during the transformation, indicating that the DCHD monomer is transformed into polymer through crystalline intermediates with lattice parameters between those of the monomer and polymer. The lattice parameter changes of the intermediates are continuous in contrast to the abrupt changes in the γ-ray polymerization of DCHD (*5*).

However, the diffraction streaking along [200] and the increase in width of the diffraction spots indicate that the transformation has certain heterogeneous characteristics. Because the lattice parameters of the intermediate phases depend on the amount of the conversion, the lengths of the error bars in Fig. 2A reflect the extent of the conversion fluctuation in the samples. The most severe fluctuations occur at 5×10^{-5} C cm^{-2}, which is also the dose at which the streaking intensity reaches a maximum (Fig. 2B). The increase in FWHM from 2° to 5° corresponds to a conversion fluctuation of 20% at 5×10^{-5} C cm^{-2}.

The total change in shape in a region is proportional to the number of polymerized molecules present. A local conversion gradient will therefore introduce a heterogeneous deformation field. The [200] streaking reveals that two-dimensional interfacial defects parallel to the (200) planes initiate and develop during the phase transformation. These two-dimensional defects are probably the result of heterogeneous deformation across an interface at which there is a local fluctuation in conversion.

To further elucidate the nature of the defects contributing to the diffraction streaking and spot broadening, we imaged the microstructural development during the phase transformation by dynamic dark-field (DF) imaging and HREM. Bend contours arise in DF imaging from heterogeneous deformation within a TEM sample. A dramatic change in the morphology of bend contours occurred during the reaction. Initially, we observed bend contours throughout the monomer crystals. We then found that new bend contours were initiated and moved through the crystal during the transformation. The final polymerized crystals were nearly free of bend contours.

The HREM images of the DCHD lattice during the phase transformation are shown in Fig. 3, A and B. The 1.2-nm (010) lattice image moved from the upper left in Fig. 3A down toward the middle in Fig. 3B. These HREM data confirm that the lattice crystallinity is retained during the phase transformation. The shift in the lattice image reflects the reorientation of the polymerizing crystal domains during the transformation. We expect that this low-dose dynamic HREM technique will provide a powerful means to study phase transformation mechanisms on a molecular level in this and other interesting polymer materials.

REFERENCES AND NOTES

1. G. Wegner, *Z. Naturforsch. Teil B* **24**, 824 (1969).
2. M. Schott and G. Wegner, in *Nonlinear Optical Properties of Organic Molecules and Crystals*, D. S. Chemla and J. Zyss, Eds. (Academic Press, Orlando, FL, 1987), vol. 2, chap. III-1.
3. J. Kaiser, G. Wegner, E. W. Fischer, *Isr. J. Chem.* **10**, 157 (1972).
4. R. H. Baughmann, *J. Appl. Phys.* **43**, 4362 (1972).
5. V. Enkelmann, R. J. Leyrer, G. Schleier, G. Wegner, *J. Mater. Sci.* **15**, 168 (1980).
6. R. H. Baughmann, *J. Polym. Sci. Polym. Phys. Ed.* **12**, 1511 (1974).
7. M. Dudley, J. N. Sherwood, D. Bloor, D. J. Ando, *J. Mater. Sci. Lett.* **1**, 479 (1982).
8. M. Dudley, J. N. Sherwood, D. J. Ando, D. Bloor, *Mol. Cryst. Liq. Cryst.* **93**, 223 (1983).
9. R. Sinclair and M. A. Parker, *Nature* **322**, 531 (1986).
10. R. J. Young and J. Petermann, *J. Polym. Sci. Polym. Phys. Ed.* **20**, 961 (1982).
11. R. T. Read and R. J. Young, *J. Mater. Sci.* **19**, 327 (1984).
12. P. M. Wilson and D. C. Martin, *J. Mater. Res.* **7**, 3150 (1992).
13. We grew the DCHD monomer single crystals (2 mm wide and 2 to 3 cm long) by slowly evaporating chloroform solution saturated with DCHD at room temperature for nearly 1 month. These crystals were embedded in an epoxy matrix and then sectioned (nominally 100 nm thick) perpendicular to the [001] direction with a Reichert Ultracut FC4E microtome. We also prepared samples by evaporating dilute DCHD-chloroform solutions of 0.01% DCHD (by weight) on amorphous carbon films.
14. V. Enkelmann, G. Schleier, G. Wegner, H. Eichele, M. Schwoerer, *Chem. Phys. Lett.* **52**, 314 (1977); P. A. Apgar and K. C. Yee, *Acta Crystallogr. Sect. B* **34**, 957 (1978).
15. D. T. Grubb, *J. Mater. Sci.* **9**, 1715 (1974).
16. R. T. Read and R. J. Young, *ibid.* **16**, 2922 (1981).
17. R. J. Young and P. H. Yeung, *J. Mater. Sci. Lett.* **4**, 1327 (1985).
18. The video digitizer is a Scion Video Image 1000 with a NuBus card installed in a Mac II. The image-processing software is Image from the National Institutes of Health, which is available by anonymous FTP from zippy.nimh.nih.gov. Our version was modified for fast Hartley transforms by A. Reeves of Dartmouth College and further modified by J. Mansfield and D. Crawford of the University of Michigan.
19. The work was supported by the College of Engineering at the University of Michigan, the Michigan Memorial-Phoenix project, and the National Science Foundation (NSF) through grant DMR-9024876. We thank J. S. Moore for help in synthesizing the DCHD monomer and the staff of the Electron Microbeam Analysis Laboratory of the University of Michigan. D.C.M. also thanks the NSF for a National Young Investigator award.

30 November 1992; accepted 1 March 1993

Secondary and Tertiary Structural Effects on Protein NMR Chemical Shifts: An ab Initio Approach

Angel C. de Dios, John G. Pearson, Eric Oldfield*

Recent theoretical developments permit the prediction of ^{1}H, ^{13}C, ^{15}N, and ^{19}F nuclear magnetic resonance chemical shifts in proteins and offer new ways of analyzing secondary and tertiary structure as well as for probing protein electrostatics. For ^{13}C, ϕ,ψ torsion angles dominate shielding for Cα and Cβ, but the addition of hydrogen bonding and electrostatics gives even better accord with experiment. For ^{15}N^{H}, side chain (χ^1) torsion angles are also important, as are nearest neighbor sequence effects, whereas for ^{1}H^{N}, hydrogen bonding is particularly significant. For ^{19}F, weak or long-range electrostatic fields dominate ^{19}F shielding nonequivalencies. The ability to predict chemical shifts in proteins from known or test structures opens new avenues to structure refinement or determination, especially for condensed systems.

It has been known for more than 20 years (*1, 2*) that the folding of a protein into its native conformation causes large ranges of nuclear magnetic resonance (NMR) chemical shift nonequivalencies to be introduced—about 10 ppm for ^{13}C (*2, 3*), 30 ppm for ^{15}N (*4*), and 15 ppm for ^{17}O (*5*) and ^{19}F (*6*). However, surprisingly little progress in computing such chemical shifts from known solid- or liquid-state structures has been made, for without these nonequivalencies modern multidimensional NMR studies of protein structure (*7*) would not be possible. An understanding of the origins of chemical shifts is expected to lead to new ways of determining, or at least refining, protein structure.

In principle, chemical shifts can be computed by using ab initio techniques (*8–10*), but full ab initio computations on structures with 1000 atoms or more are not currently feasible. However, it seems unreasonable to suppose that the effects of *all* atoms would need to be incorporated into a chemical shielding calculation because nuclear shielding is fundamentally a local phenomenon. We show that good values for ^{1}H, ^{13}C, ^{15}N, and ^{19}F folding-induced shielding can be obtained from quantum chemical methods in which we separate the total shielding, σ_t, into three parts:

$$\sigma_t = \sigma_s + \sigma_l + \sigma_0 \tag{1}$$

The short-range contribution, σ_s, contains shielding contributions that can best be evaluated through full ab initio calculation. The long-range contributions are divided into electrostatic (σ_l) and magnetic (σ_0) contributions and can be evaluated in several ways. Examples of σ_s would be the dependencies of the shielding on torsion angles, bond lengths, bond angles, and strong hydrogen bonding. Sites in helical or sheet segments normally have characteristic ϕ,ψ torsion angles, and the changes in shielding due to these geometrical parameters are caused by the changes in the electronic wave functions near the site of interest, which necessitates full ab initio calculation. Fortunately, these effects propagate through the bonding framework and are therefore very short range. As a result, one need take into account only the local geometry so that only a small number of atoms require basis functions.

For proteins, the external electrical charge field for evaluating σ_l is generated by

---

Department of Chemistry, University of Illinois at Urbana-Champaign, Urbana, IL 61801.

*To whom correspondence should be addressed.